SETI INSTITUTE

Center for the Study of Life In The Universe
2035 Landings Drive
Mountain View, Ca 94043–0818
(650) 961–6633

FINAL REPORT

to
NASA Goddard Space Flight Center
For NASA Research Grant NAG5–12658 Entitled:

"Stimulated Mid-Infrared Luminescence Experiment: Contribution to the Study of Pre–Earthquake Phenomena and UV Absorption by Interstellar Dust"

Friedemann Freund, Principal Investigator

Period of Performance: April 1, 2002 to March 31, 2003

Date Submitted: April 16, 2004

Co-investigators:
Minoru M. Freund (Wright-Patterson Air Force Research Laboratory)
Si-Chee Tsay (GSFC)
Dimitar Ouzounov (SSAI/GSFCS)

WORKING HYPOTHESIS

The work performed under this proposal is based on the experimentally supported observation – or inference – that a small fraction of the oxygen anions in silicate minerals in igneous and high-grade metamorphic rocks on Earth may not be in the usual 2- oxidation state, O^{2-}, but in a higher oxidation state, as O^{-}. If this is true, the same would likely apply to the fine dust that fills the diffuse interstellar medium.

An O^{-} in a matrix of O^{2-} represents a defect electron in the valence band, also known as positive hole or p-hole for short. When two O^{-} combine, they undergo spin-pairing and form a positive hole pair, PHP (Freund et al. 1993). Chemically speaking a PHP is a peroxy bond. In an oxide matrix a peroxy bond takes the form of a peroxy anion, O_2^{2-}. In a silicate matrix it probably exists in the form of peroxy links between adjacent [SiO_4] tetrahedral, $O_3Si/^{OO}\backslash SiO_3$. From a physics perspective a PHP is an electrically inactive point defect, which contains dormant electronic charge carriers. When the peroxy bond breaks, p-hole charge carriers are released. These p-holes are diffusively mobile and spread through the O 2p-dominated valence band of the otherwise insulating mineral matrix (Freund 2002).

Work Plan

As part of the work performed under this proposal we conducted experiments designed to shed light on processes, which are predicted to occur when p-hole charge carriers are activated:

1. increase electrical conductivity;
2. lead to the appearance of a positive surface charge;
3. lead to hole-hole recombination luminescence in the mid-IR, around 10-12 μm.

Introduction

There are three known ways to activate the PHPs and generate p-hole charge carriers :

(1) by heating to temperatures of 400-500°C (Freund 2003)
(2) by mechanical deformation and
(3) by hard UV irradiation.

In the context of this study only processes (2) and (3) are of interest.

Mechanical deformation under high levels of stress pervasively generates dislocations and causes them to move through the mineral grains. The number of dislocations formed is very high. Reported typical values are of the order of 10^{12}–10^{15} linear centimeters per cubic centimeter volume (Hanson and Spetzler 1994). As the dislocations sweep through the crystal matrix during deformation, they intercept PHPs and are predicted to release p-holes.

UV light in the energy range that reaches or exceeds the energy need to electronically excite the oxygen in the peroxy bond is also expected to break the PHPs and to cause the release of p-hole charge carriers. The absorption edge leading to the first excited state of the peroxy oxygen lies around 8.9 eV (Ricci et al. 2001).

Mechanical deformation experiments have been carried out at the Geophysical Laboratory, Carnegie Institution of Washington, in collaboration with Dr. Yingwei Fei, and at the Department of Civil Engineering, San Jose State University, in collaboration with Dr. Akthem al-Manaseer. The IR emission spectra have been measured in collaboration with Dr. Zhengming Wan, UC Santa Barbara.

UV excitation experiments have been carried out at the NIST Synchrotron Source in Gaithersburg, MD, in collaboration with Dr. Mitchell Furst. The UV-stimulated IR emission spectra have been measured in collaboration with Dr. Zhengming Wan, UC Santa Barbara.

Results

Electrical Conductivity

To see the effect of plastic deformation on the d.c. electrical conductivity of igneous rocks we performed a series of measurements using Sierra White granite from Raymond, CA, and Blue Pearl labradorite from Larvik, Norway. We measured (1) the change in the electrical conductivity of the rock undergoing plastic deformation between two cylindrical pistons and (2) the change in the electrical conductivity of the rock outside the volume undergoing plastic deformation. Variant (2) was designed to test the prediction that, when p-hole charge carriers are activated in a highly stressed volume of rock, they will flow out of the "source volume" and affect the electrical conductivity in the surrounding unstressed rock.

Figure 1 (right) shows a typical set of results of an experiment carried out according to protocol (1). The sample consisted of a slab of air-dry granite, 6 mm thick, 20 x 20 cm^2, loaded centrally via two 11.5 cm diameter steel pistons, which also served as the electrodes. During loading d.c. voltages were applied in 100 V steps from 0–1000V, each step lasting 30 sec. The load was increased linearly with time as shown in **Figure 1** (left). The slab failed after 37 min at 17 kNewton/cm^2.

Initially, a small current was flowing through the rock. The response was ohmic. As the load increased, the conductivity increased rapidly up to about 1/2 of the load to failure. The response remained ohmic. At higher loads the current tended toward a steady state value, suggesting that the conductivity reached steady state. The steady state value did not strongly depend on the number of cracks so long as the pieces stayed together. Eventually, failure led to crumbling of the central part of the slab accompanied by a sudden release of stresses and an instant drop in the overall conductivity.

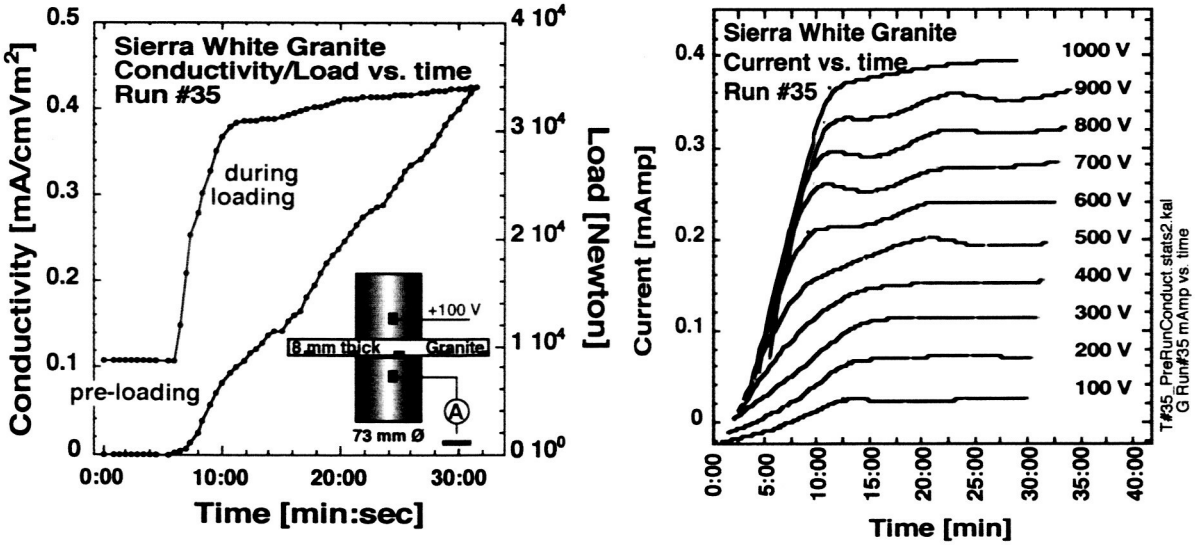

***Figure 1** (left): Load versus time up to failure at 17 kNewton/cm^2 and increase of the conductivity as a function of loading. The insert shows the experimental set-up with the pistons acting as electrodes. (right): Increase of the current flowing through the highly stressed granite at different applied voltages, indicating that the stress activates charge carriers and that the response is ohmic.*

Figure 2a shows an experimental set-up according to protocol (2), where we used again the pistons as one pair of electrodes to measure the current through the volume of rock actively undergoing deformation and added a second pair of electrodes to measure the current flowing through the rock outside the stressed volume. **Figure 2b** shows the two currents as a function of the load at a constant load increase up to

failure. As in the case depicted in **Figure 1**, the current through the stressed rock volume (blue curve, right hand scale) increases rapidly after application of the load. It seems to tend toward a plateau only to increase again about halfway into the run, shooting up to high values just before failure. The current through the unstressed rock volume also increases very rapidly upon application of the load but then goes into strong fluctuations and decreased to about background values halfway into the run.

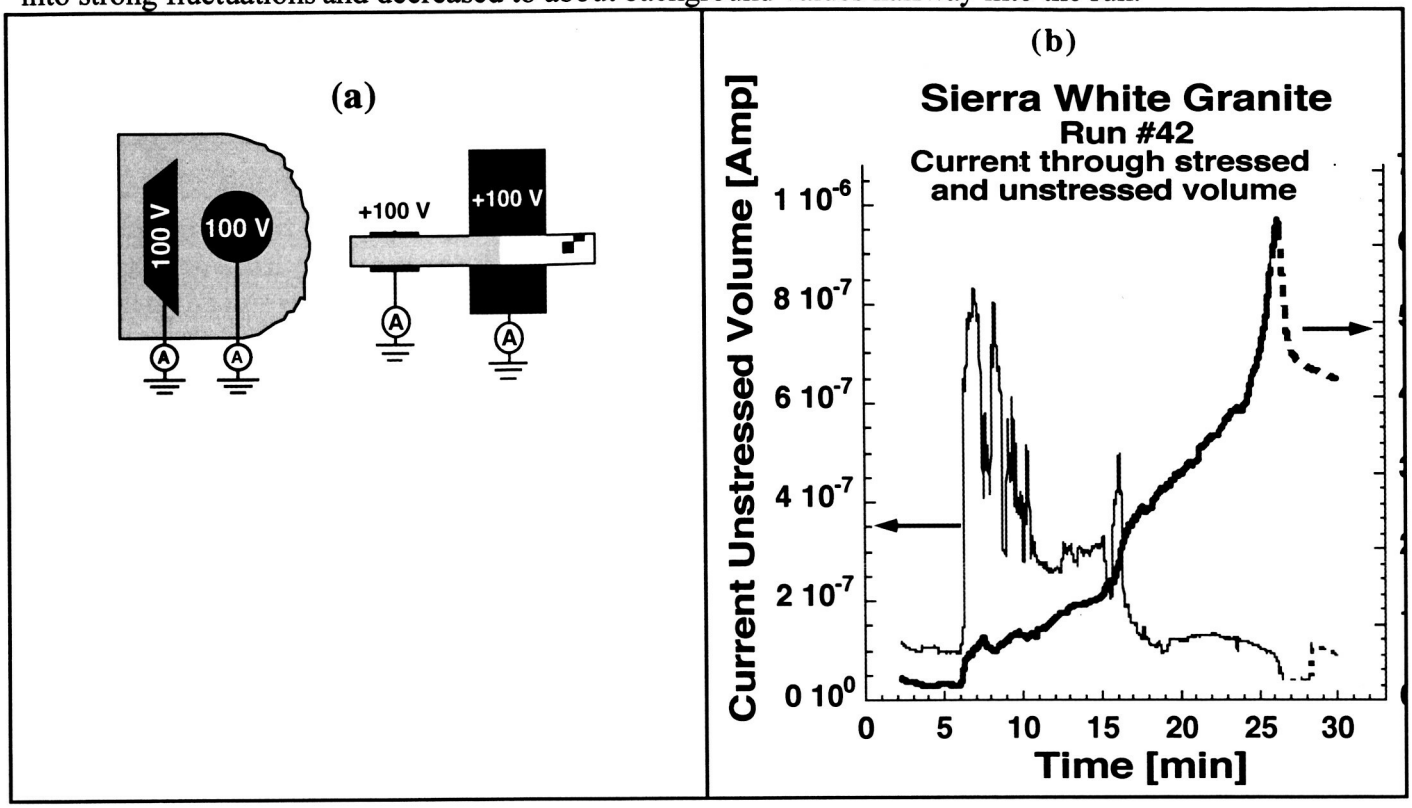

*The experiment depicted in **Figure 2** suggests that charge carriers activated in the rock volume under active stress, e.g. in the rock volume between the pistons, are capable of flowing out of the "source volume" and affect the conductivity of the surrounding unstressed rock.*

To further study the outflow of charge carriers we designed another variant as depicted in **Figure 3** from a photograph taken at the Mechanical Test Station at SJSU. We used 30 x 30 cm^2 rock tiles, 9.3 mm thick. As sketched in **Figure 4a** the two pistons served as one electrode, electrically insulated them from the frame and applying +100 V to both. The outer periphery of the tile was grounded via conductive Cu tape.

Figure 4b shows that, as soon as load applied, the current flowing from the pistons to the periphery increases in a stepwise fashion and continues to increase up to about halfway through the experiment. Given the thickness of the rock tile and its lateral size the residual stresses the emanate from the central "source volume" are relatively small. The fact that nonetheless the current flowing from the central pistons to the periphery increases as the load is applied ca be taken as a strong indication of an outflow of charge carriers from the volume between the pistons to the surrounding unstressed rock.

Control experiments with plate glass of the same dimensions as the rock tiles failed to produce a measurable increase of the current from the central pistons to the periphery. This is consistent with the fact that regular glass does not seem to contain any PHPs and does lead to the activation of p-hole charge carriers by the application of stress. To further improve these measurements we built a sturdy metal frame to confine the rock tiles laterally. This prevented the files from breaking apart and allowed us to apply significantly higher loads before failure.

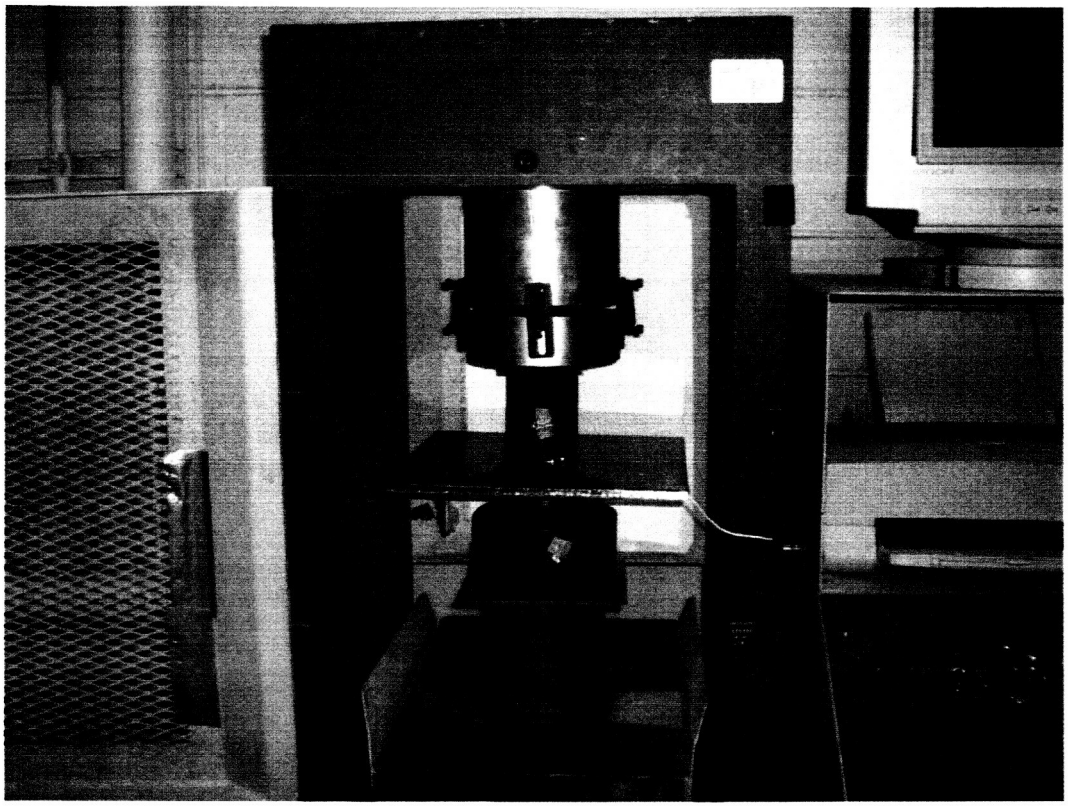

Figure 3**: Rock tile mounted in the press at San Jose State University, prepared for the stress-induced conductivity experiment depicted in **Figure 4.

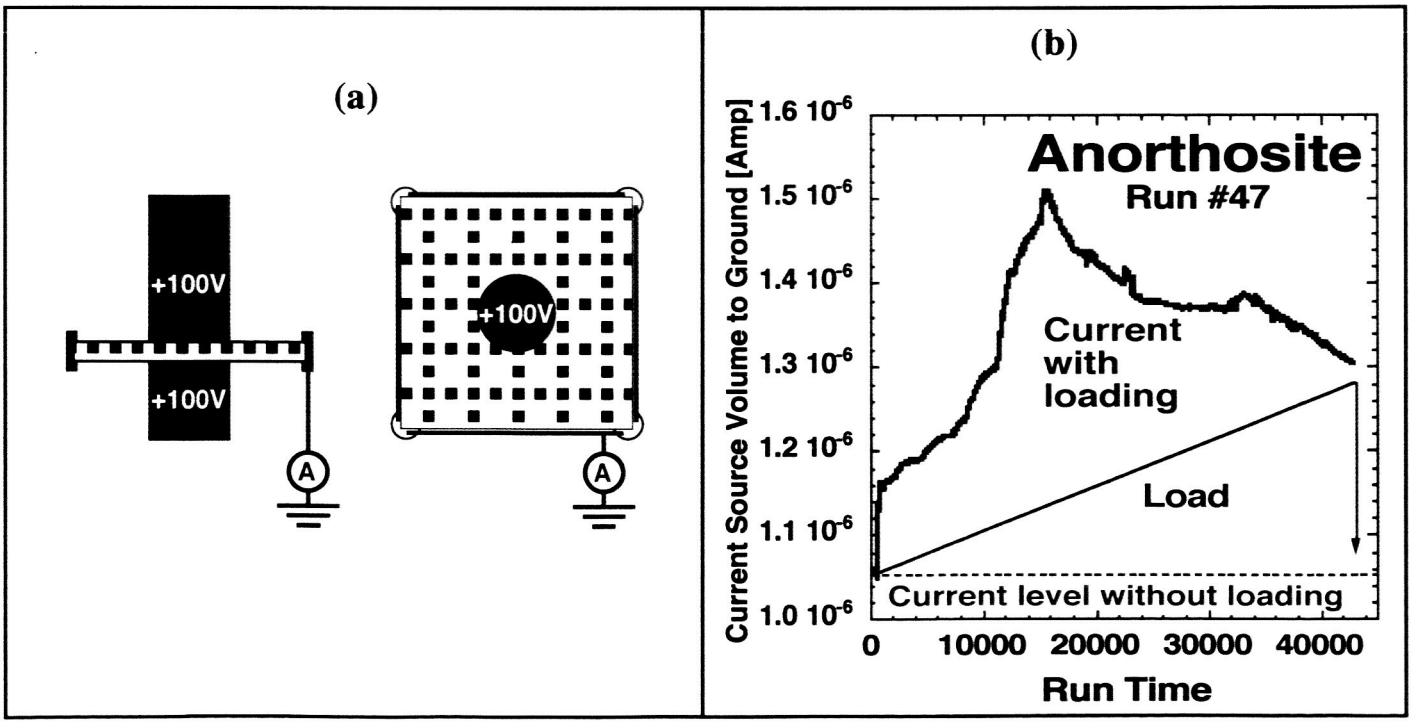

***Figure 4**: Stress-enhanced electrical conductivity experiments **(a)** schematic lay-out in side view and top view, and **(b)** current flowing from the central "source volume" of rock between the pistons, biased at +100 V, to the grounded periphery, as a function of the load during linear loading.*

Positive Surface Charges

A limitation of the current measurements as described until now is that we always impose an external electric field. However, if the rock volume between the pistons acts as "source" from where p-holes flow out into the surrounding rock, we should see self-generated electric potentials across the rock.

We set up an experiment to measure (i) the potential difference between the pistons and a capacitor plate on the rock surface, and (ii) the current flowing from the rock into ground or from ground into the rock. We used two slightly different electrode configurations. Instead of the round pistons acting on the center of the tile we applied the load via a pair of rectangular pistons (22 x 4 cm^2). We insulated three edges of the tile from the frame but applied a Cu stripe to one edge as the ground contact.

For the first configuration, depicted in the insert in **Figure 5a**, we inserted 0.8 mm plastic sheets between the pistons and the tile. By also insulating the pistons from the rest of the press by 0.8 mm plastic sheets, we turned them into one plate of a capacitor with the rock forming the other plate. We then created a second capacitor by placing a sheet of aluminum (28 x 8 cm^2, 1 mm thick) on one side of the tile, insulating it from the rock by a 0.8 mm plastic sheet. We measured the voltage between the two capacitors using a Keithley 617. Grounding the Cu stripe along the edge through a Keithley 486, we measured the current flowing into or out of the rock.

For the second configuration, depicted in the insert in **Figure 6a**, we used an aluminum sheet capacitor (28 x 8 cm^2, 1 mm thick) but placed both pistons in direct metallic contact with the tile but insulated them from the press by means of 0.8 mm plastic. Thus, we allowed any charges, which the stressed rock would generate, to flow into the steel pistons. We measured (i) the voltage between the pistons and the aluminum sheet capacitor using a Keithley 617, and (ii) the ground current using a Keithley 486.

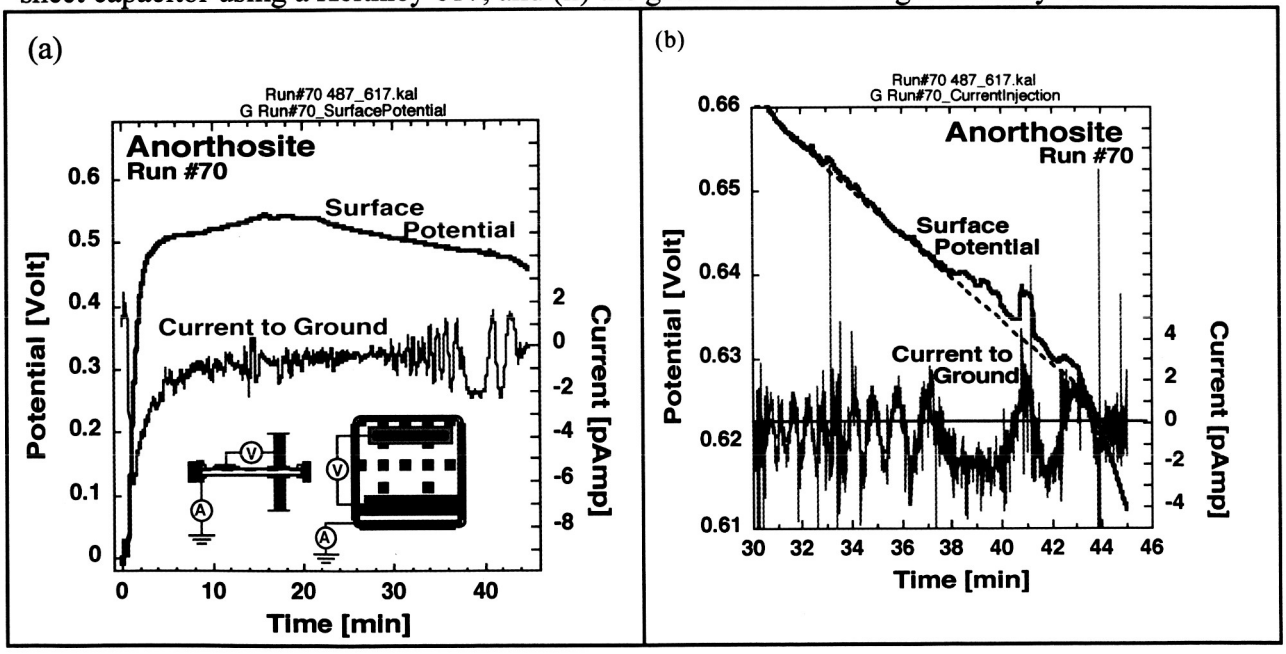

***Figure 5a**: Load versus time plot and two-capacitor configuration to determine the self-generated electric field and currents when the rock is stressed without any externally applied voltage; **(b)** Surface potential (red) building up rapidly upon loading between the unbiased pistons and the capacitor, and current (blue) flowing into and out of the rock from ground.*

With the first electrode configuration we observe the build-up of a potential difference between the two capacitors, e.g. the voltage that develops between the stressed rock and the unstressed rock outside the pistons. As Figure 10a shows, the potential turns positive as soon as the load is applied, reaching rapidly 500 mV and later 550 mV about half way into the run. At the time of the rapid rise of the potential

difference a small current is drawn into the rock from ground. Its maximum is about –6 pAmp and coincides with the steepest slope of the voltage versus time curve. Such a current represents the number of charge carriers flowing into or out of the rock in response to the generation of p-holes in the "source volume" and their spreading into the unstressed rock. Soon thereafter the current drops to zero but there are signs of oscillations toward the end of the run. At first we discounted these oscillations as noise but then noticed slight variations in the voltage versus time curve, which correlate with the potential variations.

In **Figure 5b** we have magnified the current oscillations and the corresponding portion of the voltage versus time curve. The two curves bear resemblance to the current and voltage oscillations observed during impact experiments, where they are believed to have been caused by electron injections into the rock in response to the build-up of a positive surface charge exceeding the Schottky barrier height (Freund 2002). Similarly, in the case presented here, we have to consider the possibility that the positive charge at the rock surface can reach sufficiently high values to allow electrons from ground to be injected across the metal-to-insulator interface at the contact of the Cu grounding electrode.

With the second electrode configuration we also observe a potential difference as shown in **Figure 6**. This time the potential develops between the aluminum sheet capacitor above the rock surface and the two pistons, which are in electrical contact with the "source volume" of the rock. The charge generated in the "source volume" communicates directly with the piston. It thereby becomes diluted and the maximum potential attained is about 1/10 the potential observed with the first electrode configuration where the rock had been insulated from pistons by the insertion of the 0.8 mm plastic sheets.

At the same time the current flowing from the ground into the rock is about 10 times larger, reaching 40 pAmp. Concurrent maxima and minima suggest a coupling between the current and the surface potential.

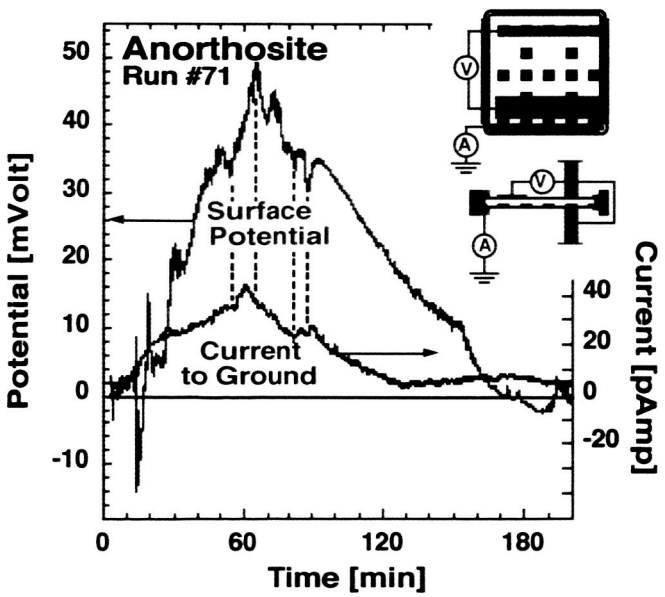

***Figure 6**: Self-generated electric field between the pistons, which are in electrical contact with the rock, and the capacitor, plus self-generated currents from to ground; Surface potential (red) and current (blue) flowing into and out of the rock from ground.*

Lastly, we conducted experiments designed to measure the formation and propagation of p-hole charge clouds relative to the fracturing of the rocks. Vallianatos and Tsanis (Vallianatos and Tsanis 1998) have described how preseismic and coseismic electrical signals are related to the rate with which rocks are deformed. Similarly during stick-slip experiments with granite cylinders, Takeuchi and Nagahama

(Takeuchi and Nagahama 2001) observed that a sharp positive voltage pulse always arrived 1-2 msec before the actual slip marked by an acoustic signal. The positive voltage was followed by a somewhat broader negative voltage.

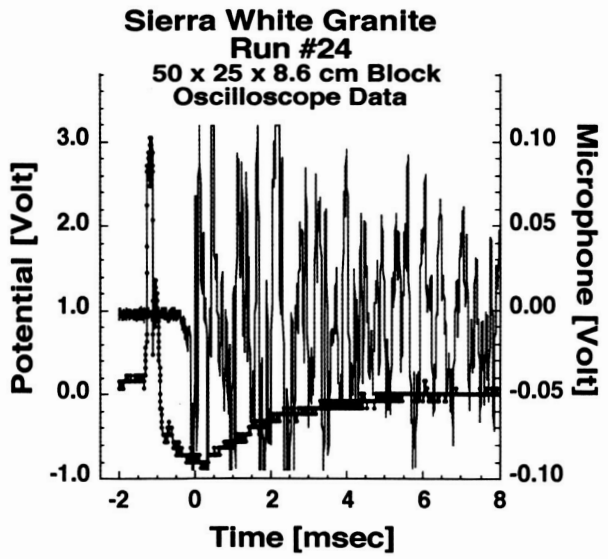

***Figure** 7: Sharp voltage pulse indicating the build-up of a surface potential (red) before the crack monitored by it acoustic signal (blue).*

For our uniaxial rock deformation experiment we set up a thick slab of granite, applied a capacitive sensor about 10 cm from the pistons and a microphone about 1 cm from the pistons. Using a 4-channel oscilloscope we used the acoustic signals from major cracks occurring during loading to record the voltage at the capacitive sensor and the acoustic wave. **Figure 7** shows a typical result: a sharp positive voltage arrived about 1.5 msec before the acoustic signal. The sharp positive voltage pulse was followed by a broader negative voltage pulse before the signal returned to the baseline.

The implications of this particular sequence of the voltage and the acoustic signals are that a mechanism exists in the deforming rock, which generates a cloud of highly mobile positive charges just before the stresses reach the level where fracture occurs. This is consistent with p-hole charge carriers being activated by dislocations which appear in ever larger number as the rock approaches catastrophic failure. This state is reached when the dislocations generated during plastic deformation reach a critical density and begin to converge into microcracks. The microcracks in turn coalesce into a major crack that initiates catastrophic rupture (Miguel et al. 2001).

Infrared Emission

First rock deformation experiments were conducted at the 1500 ton press of the Geophysical Laboratory, at constant rate of pressure increase until failure. To measure the IR emission we used a QWIP (Quantum Well Infrared Photodetectors) camera from NASA Goddard Space Flight Center with a 256 x 256 GaAs/AlGaAs array operated at $\approx$ 67K, using pumped liquid N_2, with full wells at 7.5 x 10^6 e^-/pixel, a dark current of $\approx$ 60 pA/pixel, an 8–8.5 μm bandpass filter, and F/2 ZnSe optics with a field-of-view of 9°. The QWIP camera can detect brightness temperature differences as small as 25 mK (NEΔT $\approx$ 0.025K).

As samples we used blocks of coarse-grained, porphyritic granite "Imperial Red" from the Archean Complex of South India, supplied by Gem Granites (quarry location 20 km south of Hungund, 5 km east of Ilkal at N15°55'27", E76°04'24"). The granite was selected for its high compressive strength (200 N/mm^2) and high modulus of rupture (24 N/mm^2). At a mean density of 2.615 g/cm^3, its porosity (as

measured by water absorption) is 0.07%. Two sample sizes were studied, small blocks of 9 x 9 x 13 cm^3 and large blocks of 25 x 25 x 9 cm^3. Three types of experiments were performed as illustrated in **Figure 8.**

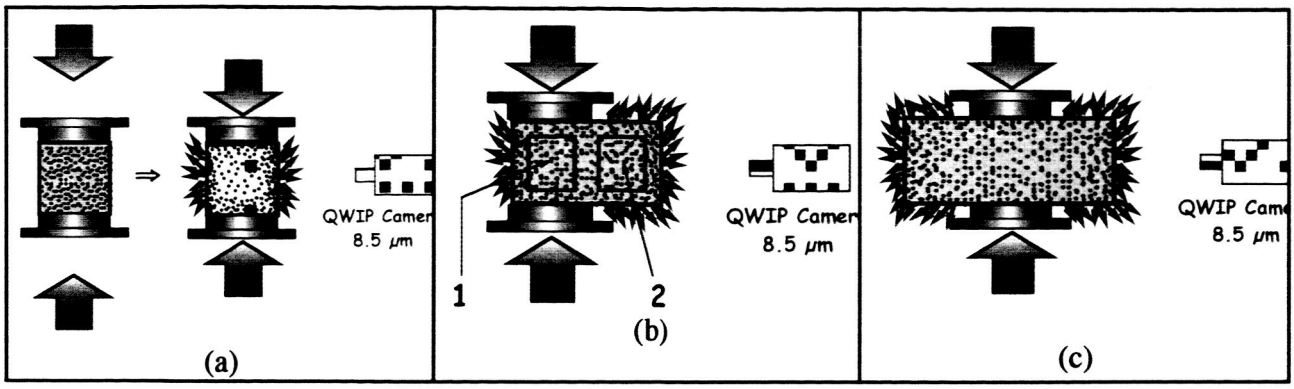

Figure 8: *Three variation of the rock deformation – IR emission experiment.* ***(a)****: deforming the entire block and recording the IR emission from its surface;* ***(b)****: deforming one half of the block and recording the IR emission from the surface of that part which undergoes deformation and from the other part which is left unstressed;* ***(c)****: deforming only the central part of a large block and recording the IR emission from its outside, unstressed surfaces.*

First, small blocks were loaded standing upright, pressing on their 9 x 9 cm^2 faces. Thus their entire volume was deformed as in **Figure 8a**. Second, same blocks were loaded lying sideways on their 13 x 9 cm^2 faces, deforming only one half as in **Figure 8b**. Third, the load was applied to a circular area at the center of the 25 x 25 cm^2 faces of the large blocks, 10 cm diameter as in **Figure 8c**. During all runs the granite blocks were electrically insulated from ground to better than 10^{12} Ω by inserting 1 mm thick hard plastic sheets between them and the piston plus base plate of the press. To screen out ambient light and stray IR radiation, the samples were surrounded by a wooden box, open toward the QWIP camera. A sheet of black foam rubber placed behind the rocks provided a constant intensity background.

During uniformly loading of the small blocks of rock (standing upright on their 9 x 9 cm^2 faces as in **Figure 8a**) the QWIP camera recorded enhanced IR emission from the front face and the edge. The IR emission began above ≈ 1/4 to 2/5 of the load to failure. The intensity of the IR emission increased approximately linearly from 20 bar to 40 bar input pressure. Above 40 bars audible internal fractures started to develop in the block, and the intensity of the IR emission from its surface began to decrease. Failure occurred shortly above 50 bars. With this experimental set-up the increase in IR emission from the rock surface may have arisen from the conversion of mechanical energy into heat through microfractures at the surface. Next we loaded only half the block (lying sidewise on its 9 x 13 cm^2 face as depicted in **Figure 8b**). We again observed an increase in the intensity of the IR emission as a function of pressure,. The IR emission from the unstressed half cannot be explained by the generation of heat through local fractures or microfractures or any other stress-induced process.

Next we loaded the central part of the large 30 x 30 x 10 cm^3 blocks as depicted in **Figure 8c**. With the outer unstressed volume acting as confinement, much higher loads to be achieved before failure.

Figure 9a/b depicts a large block in the 1500 ton press, before and after the run, photographed without the wooden box to shield the ambient visible and IR light and without the upper plastic sheet, which provided electrical insulation from the upper piston. The large plastic sheet, which provided electrical insulation from the lower base plate, is seen as a whitish surface. While the small blocks tended to fail explosively, with small chips flying up to 2 m away, the failure mode of the large blocks was less dramatic. At first, internal fractures developed within the near-cylindrical central portion. Then, hair

fissures developed, extending radially toward the surfaces. Failure occurred abruptly when massive radial fractures broke the block in several segments as seen in **Figure 9b**.

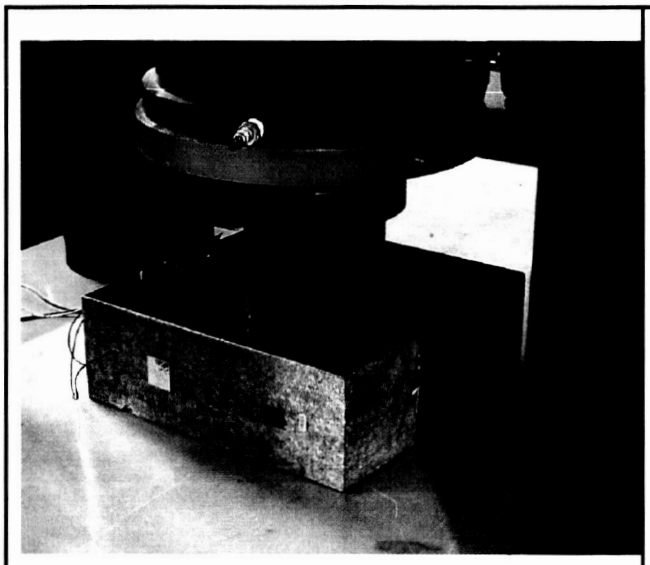

***Figure 9a**: Large granite block, 30x30x10 cm^3, in the press before the deformation under load*

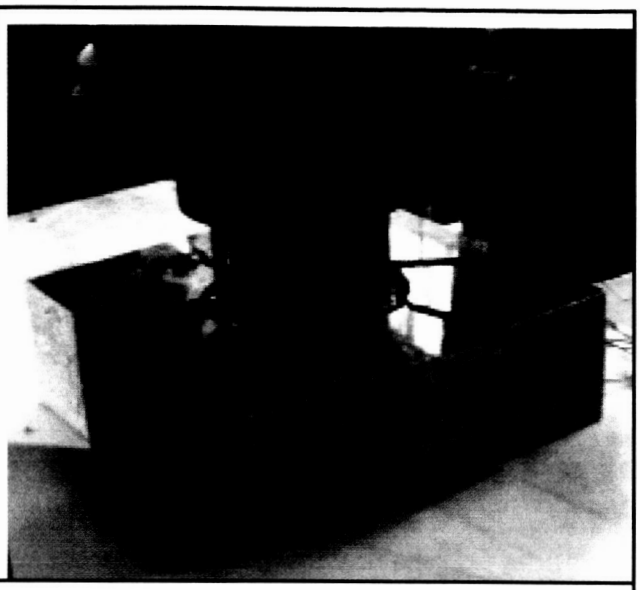

***Figure 9b**: Same large granite block after failure*

Before failure, however, the blocks seemed to emit in the mid-IR as evidenced by the QWIP images shown in **Figure 10**. The IR emission came primarily from the edges of the granite block. This is consistent with the concept of the positively charged p-hole charge carriers spreading out through the uncharged dielectric medium of the rock. Due to mutual repulsion (counteracted by Coulomb interaction with the negative charge left behind in the "source volume") they will accumulate along edges and corners. The probability for recombination and, hence, for IR emission, should be highest at these sites of maximum curvature.

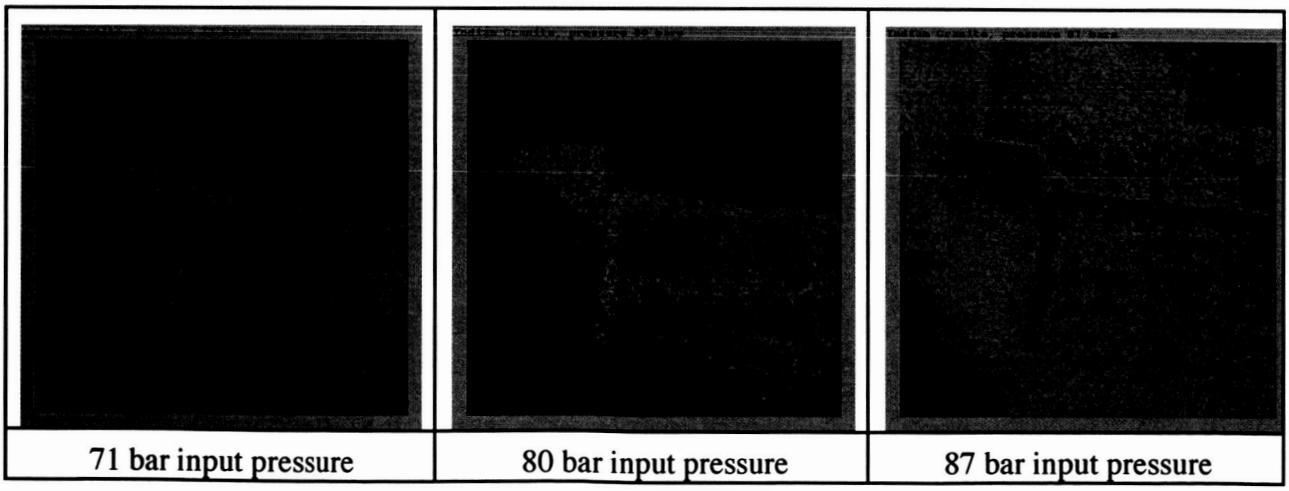

71 bar input pressure | 80 bar input pressure | 87 bar input pressure

***Figure 10**: Exemplary (uncorrected) false-color images taken during deformation of a large granite block. In the upper right hand corner the upper piston can be seen. Below is about 1/2 of the 30x30x10 cm^3 block. At the lower left is a second block of granite leaning against the main block. It shows IR emission as well, indicating that the p-holes are flowing over to the second block across a point contact. Failure at 112 bar.*

More recent rock deformation experiments were carried out at San Jose State University using blocks 30 x 60 x 7.5 cm^3 (1' x 2' x 3"). The blocks were placed between two stainless steel pistons as depicted in **Figure 11** and electrically insulated by 1 mm thick sheets of high resistance plastic (>10^{12} Ω). Though we are aware that constant strain rate experiments are the preferred mode, we loaded the rocks at a constant rate (1.5–2 kg/sec cm^2). The approximately cylindrical rock volume undergoing deformation, the "source volume", was inside the blocks, i.e. away from the edges. The periphery acted as confinement, providing a 15-35 cm thick layer of rock, which the p-hole charge carriers had to traverse in order to reach the surface. The peripheral portion was under tensile stresses along a few narrow stripes. To a good approximation the outer rock surface can be considered stress-free.

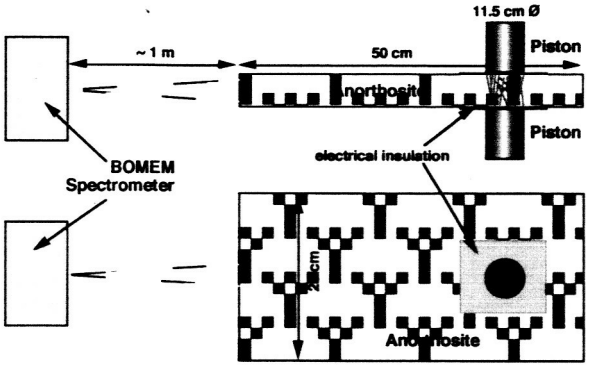

***Figure 11**: Schematic side and top views of the IR emission experiment with 50 x 25 x 7 cm^3 blocks held between two 11.5 cm diameter steel pistons and electrically insulated. The FT-IR BOMEM spectrophotometer was at a distance of ~1 m from the front 25 x 7 cm^2 face. The IR emission was collected from a circular spot of about 5 cm diameter. Details of the procedure are given elsewhere* (Wan et al. 1999).

We present mid-IR emission data from a coarsely grained Norwegian anorthosite, "Blue Pearl", a quartz-free igneous rock composed to 95+% of the Ca-rich feldspar labradorite, $Ca[Al_2Si_2O_8]$, with crystals measuring on the average 10–30 mm in size.

Obviously, when a rock is loaded at one spot as depicted in **Figure 11**, the IR emission from its front face should not change. However, this is not what we have observed. **Figure 12a** complies 10 pre-run files, each consisting of 25 scans of the FT-IR spectrometer, recorded over a period of about 4 min before loading the rock. The small drift in these spectra is due to a slight ambient temperature drift in the laboratory. The bold black curve represents the average of all pre-run files at zero load. During the run, while the load was increased at a constant rate, the IR emission spectra were continuously recorded. Failure occurred after 18 min.

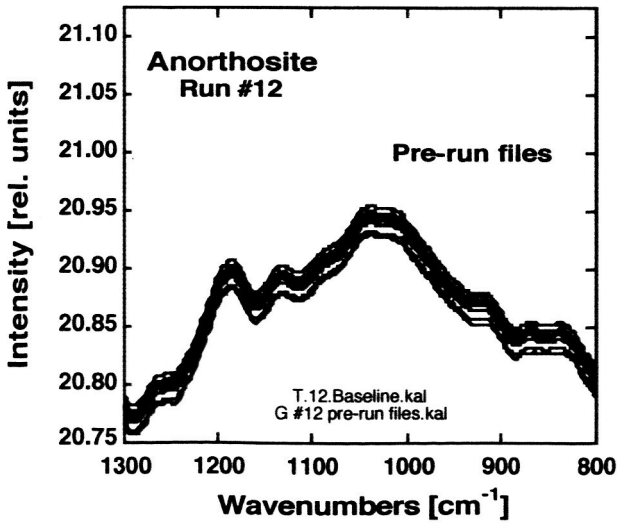

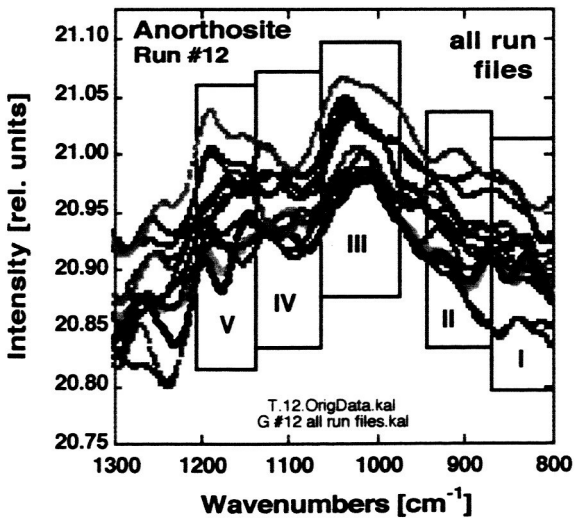

***Figure 12a**: Emission spectrum before loading during Run #12. Fine lines: 10 pre-run files recorded while the ambient temperature drifted slightly upward. Bold line: Average.*

***Figure 12b**: Full range of emission spectra recorded during loading of Run #12, while the temperature continued to drift upward. Note change of the emission spectra upon loading.*

Figure 12b shows that the IR emission from the front face changes as load is applied 35 cm away from the emitting surface at the center of the block. The changes occur near-instantly, ruling out that they are due to frictional heat diffusing from the "source volume" to the surface. The changes affect the intensity distribution over the entire spectral range displayed. The data used to produce **Figure 12b** comprise all 45 files, each of 25 scans, collected over about 18 min and averaged in groups of 3 to give a total of 15 files. The boxes I–V outline five ranges of interest. The large number of spectra improves the signal-to-noise ratio and allows us to see trends. To show as an example how the emission intensity evolves with load, we plot in **Figure 13** the intensity variations in Box II, uncorrected for the temperature drift.

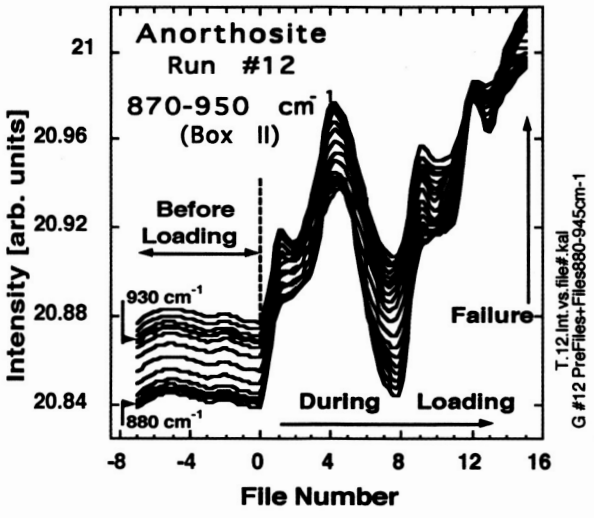

Figure 13 demonstrates that, while the intensity in the 870–950 cm^{-1} window is constant before loading, it increases as soon as load is applied. The intensity oscillates up to the time of failure. We observed oscillations during every run during our 2002 and 2003 measurements: the IR intensity always rose relatively sharply at the beginning and then either leveled off or began to oscillate.

***Figure 13**: Intensities in the 870–950 cm^{-1} window delineated in **Figure 12b**, plotted versus the file number for the pre-run and run files for Run #12. The file numbers are about equal to the number of minutes after start.*

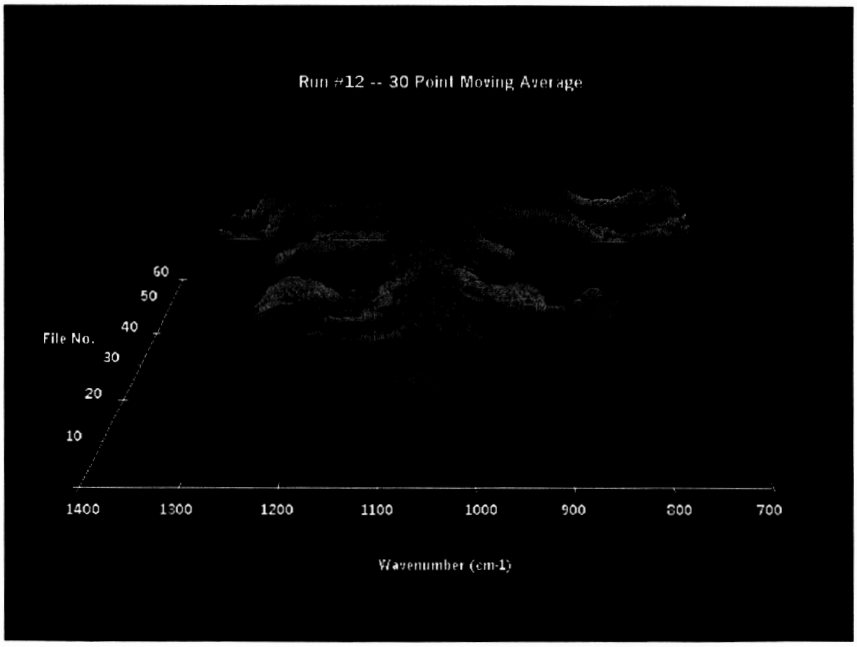

***Figure 14:** 3-dimensional projection of all Run #12 spectra #12, uncorrected for temperature drift.*

The oscillations are still very poorly understood. We believe tha they arise from the electrostatic field, which builds up that the surface when p-holes arrive. The electrostatic field prevents further inflow of p-holes until it dissipates by some as yet unkown mechanism. **Figure 14** shows the same data as in **Figure 12a/b** in a 3-D representation. The pre-run files are in the front;

Though the number of experiments performed so far is still limited, it appears certain that several emission bands increased in intensity with increasing load. Bands, which are absent or weak in the pre-run spectra, appeared as soon as the load was applied. This observation, if confirmed by more experiments, points to IR emission bands, which are due to the deactivation of the vibrationally excited PHPs forming at the rock surface through hole-hole recombination.

This leads to yet another consequence: IR emission bands may arise from Si–O and Al–O bonds that become activated during thermalization of excited O^-–O^- bonds. The rationale is as follows: If vibrational excess energy flows from the highly excited O^-–O^- bonds to neighboring Si–O and Al–O bonds, theory predicts that this process is sensitive to temperature changes. Normally the coupling between the vibrationally excited O^-–O^- bond and the neighboring Si–O and Al–O bonds is strong because the vibrational modes are separated in frequency space by ~200 cm^{-1}, close to the mean thermal energy kT at $T \approx 300K$. By lowering the temperature we expect to decrease the coupling and thereby allow the energy from the excited O^-–O^- bond to flow in a more "orderly" way over to the adjacent Si–O and Al–O bonds.

To test this hypothesis we set up run #22 with a block of anorthosite, which had been cooled to –10°C. The experiment was done as described for run #12, i.e. at room temperature in air. The spectra were recorded after the rock surface had stopped frosting over. The core of the block was still cold. Before starting the data collection we wiped the condensing water off the face of the rock facing the BOMEM FT-IR photospectrometer. A total of 45 spectra with 25 scans each were recorded in succession, while the block was loaded at a constant rate up to failure.

Figure 15a shows all 45 spectra, averaged in groups of 3. The bold black line traces the average of all spectra. The color-coded boxes I, II, and III designate spectral windows, in which significant changes in the IR emission intensities were observed as shown in **Figure 15b**.

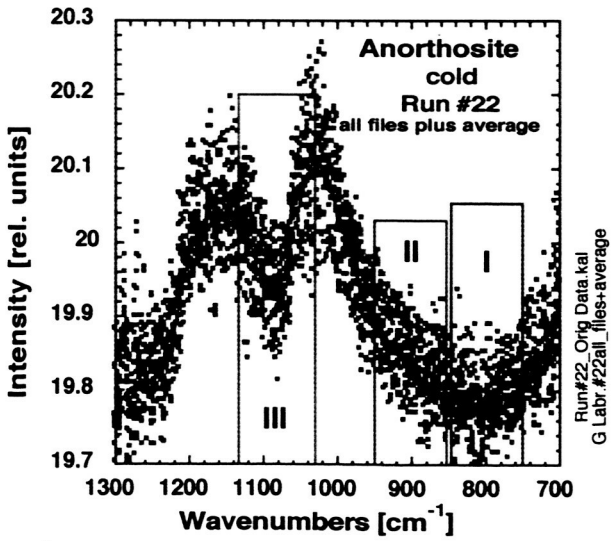

*Figure 15a: Superposition of all data from 45 spectra recorded during Run #22. Bold black line: average. Boxes I, II, and III: spectral windows of special interest (see **Figure 12b**).*

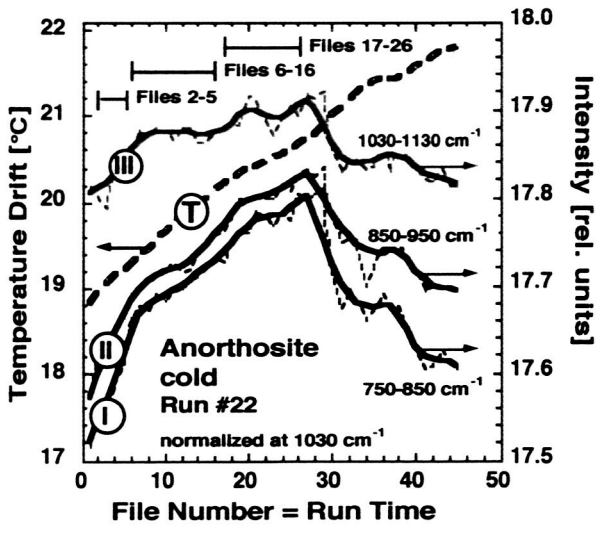

*Figure 15b: Smoothed intensities in the spectral windows as outlined by I, II and III in **(a)**. Fine lines: unsmoothened data. Bold dotted line: T–drift. Rock failure at file #45.*

In **Figure 15b** we plot the temperature drift (left scale) and the IR intensity (right scale) after normalizing all intensities to 1030 cm^{-1}, i.e. to the maximum of the emission in this spectral region. The three bold colored lines show the averaged intensities in the three boxes I, II and III as a function of file number, i.e. time during loading. The fine lines show the unsmoothened data. The horizontal bars in the upper portion delineate three distinct regions with different slopes. Initially (files #2–5) the intensity increases steeply. Later (files #6–16) the intensity increases somewhat less steeply. Still later (files #17–26) the intensity tends toward saturation. After the maximum at file #26 the IR intensity decreased but did not recover.

UV Irradiation and Stimulated IR Emission

As part of this project we also set out to study the activation of positive hole charge carriers in mafic and ultramafic minerals and in igneous rocks by hard ultraviolet (UV) radiation.

Our working hypothesis was that the dormant positive hole pairs (PHP) can be activated by hard UV radiation. The PHPs are then expected to release positive hole charge carriers (p-holes), which spread through the rock as defect electrons in the O 2p-dominated valence band of the constituent minerals.

We were interested in using UV activation to study whether p-hole charge carriers spread from their point of origin, e.g. from the UV-irradiated surface, through the unirradiated portions of the rock. If they do, the p-holes are expected to appear on the other side of a thick, UV-irradiated sample. At the surface of the other side they are expected to recombine to PHPs. The p-hole recombination is exothermal. The release of energy is expected to lead to vibrationally excited O-O bonds. Such excited O–O bonds will de-activate

(i) by emitting mid-IR photons at the characteristic wavelengths of the O–O vibrations

(ii) by transferring energy into neighboring Si–O and Al–O bonds, causing them to emit at the wavelengths of their respective (Si,Al)–O stretching and bending vibrations.

To test this hypothesis we used the Synchrotron Ultraviolet Radiation Facility SURF III at the National Institute of Science and Technology (NIST), Gaithersburg, MD. We irradiated 1 cm diameter spots on one side of a 0.7 cm thick synthetic MgO single crystal and 1 cm diameter spots on one side of 2-3 cm thick slabs of natural granite and dunite. The granite was light gray from the Sierra Nevada, California, from the Raymond quarries near Fresno, CA. It consisted of roughly 1/3 quartz, 1/3 Na-rich feldspar and 1/3 Ca-rich feldspar with a few accessory minerals. The dunite came from the Northern Cascades, Washington, and consisted of over 95% of green olivine of upper mantle provenance.

We used a MIDAC IR emission spectrometer to measure the change in the IR radiation emitted from the opposite sides of the MgO single crystal and of the slabs of rocks as we switched the UV beam on and off. The experiments were conducted at ambient temperature in air. The outlay of the experiment is shown schematically in **Figure 16**.

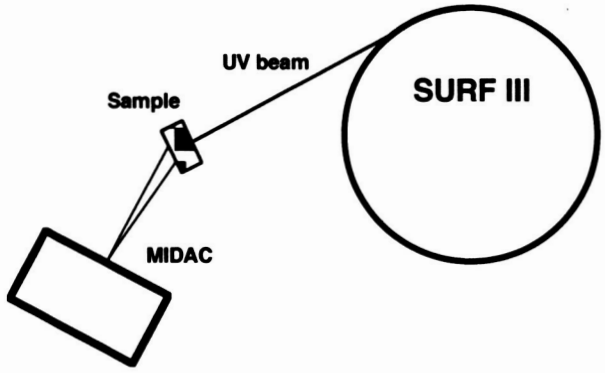

***Figure 16**: Schematic of the UV-stimulated IR emission experiment at the NIST Synchrotron source.*

Figure 17a/b shows the intensity of the IR emission as a function of time for a large number of narrow wavelength bands over the 700–1400 cm^{-1} (14.2–7.1 μm) range. The overall downward trend is due to a drift of the ambient room temperature. The UV beam was switched on between the time steps 120–245.

(a)

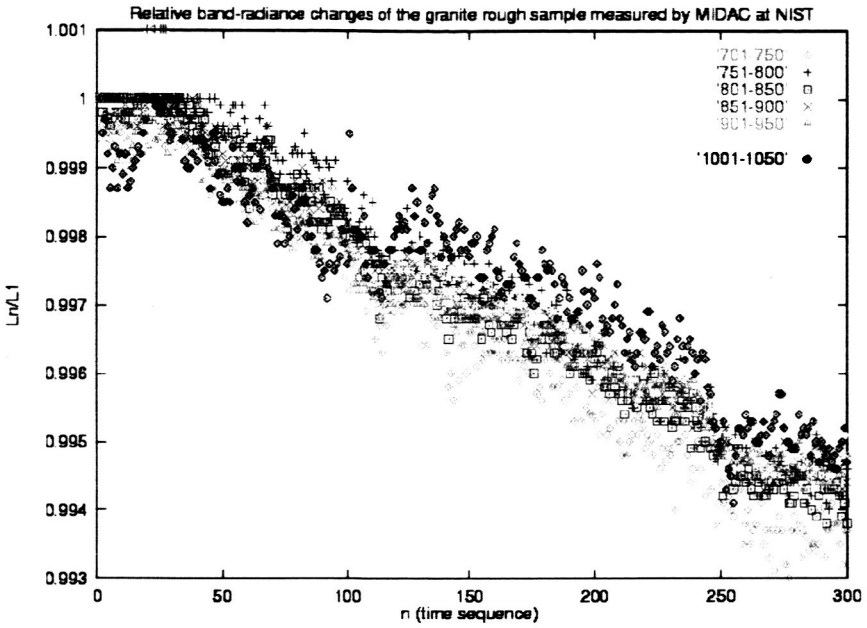

(b)

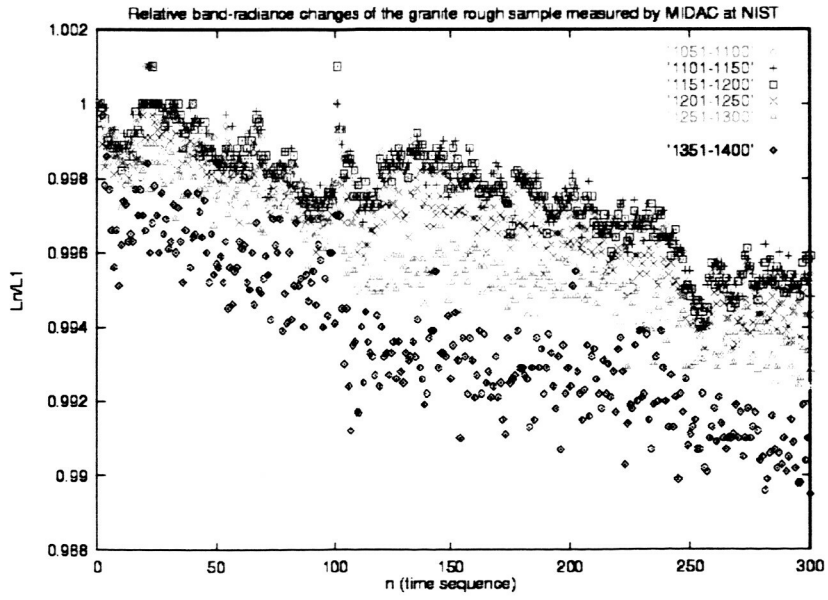

***Figure 17**: IR emission intensity recorded in a large number of narrow wavelength bands between **(a)** 700–1050 cm^{-1} (14.2–9.5 μm) and **(b)** 1100–1400 cm^{-1} (9–7.1 μm). The downward trend is due to a drift of the room temperature. The UV beam was on between time steps 120–245.*

In the following we present the analysis of the IR emission data from a Sierra White granite. The data from **Figure 17** in the time step windows 90–100 and 120–240 were converted into spectra and averaged. In **Figure 18a** the spectra obtained are labeled "UV beam off" and "UV beam on".

Figure 18b shows the difference between the two spectra and two straight lines representing a linear fit to the background. **Figure 18c** shows the baseline-corrected IR emission spectra. The blue arrows indicate bands that are considered candidates for the UV-stimulated IR emission. The dashed portion of the spectrum between 1400–1300 cm^{-1} is believed to be contaminated by the emission of H_2O in the ambient air. The relatively strong dashed band around 950 cm^{-1} is a result of the fitting procedure, though a weak emission feature at 925 cm^{-1} seems to be present as indicated by the small band in **Figure 18b**.

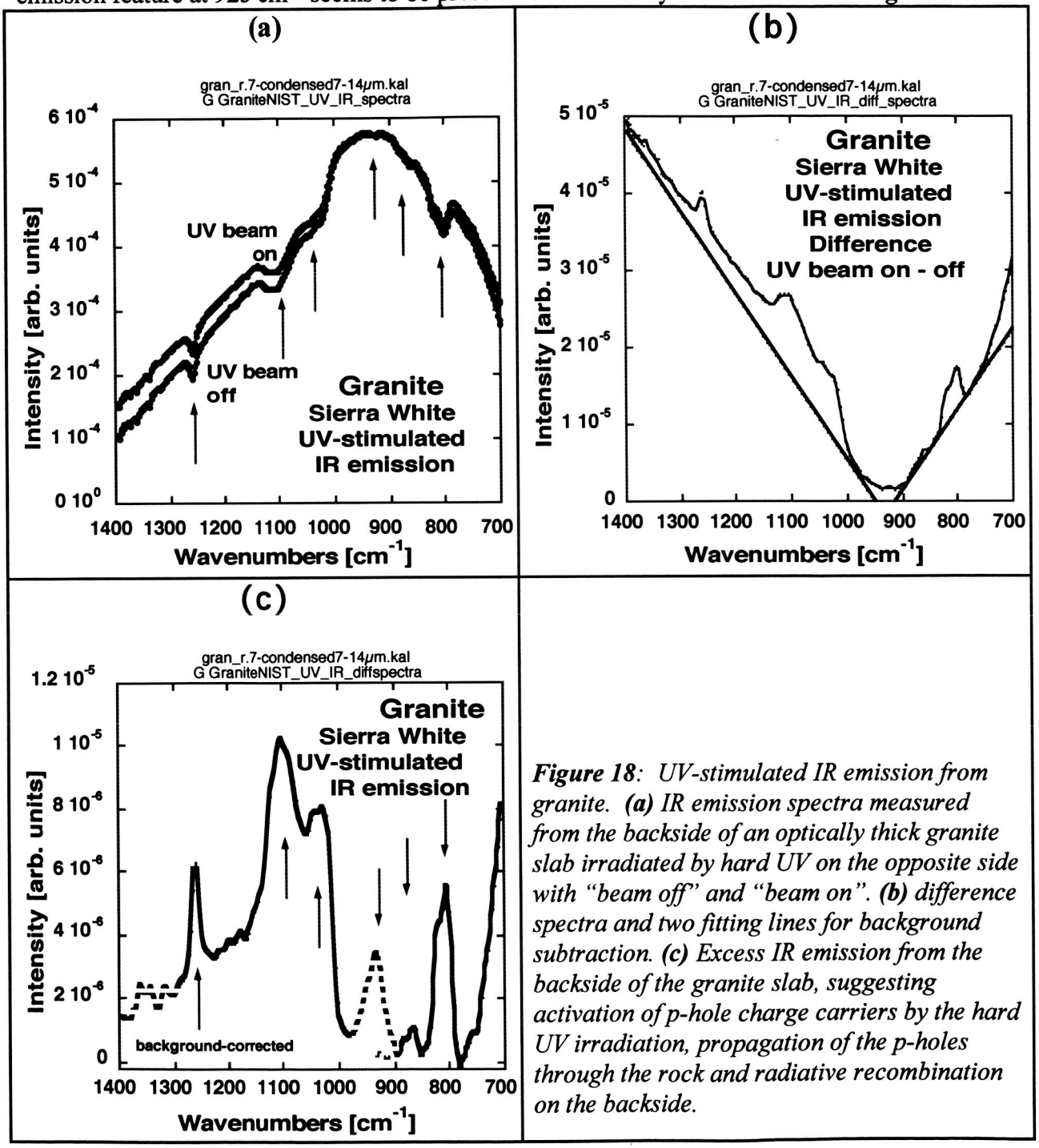

*Figure 18: UV-stimulated IR emission from granite. **(a)** IR emission spectra measured from the backside of an optically thick granite slab irradiated by hard UV on the opposite side with "beam off" and "beam on". **(b)** difference spectra and two fitting lines for background subtraction. **(c)** Excess IR emission from the backside of the granite slab, suggesting activation of p-hole charge carriers by the hard UV irradiation, propagation of the p-holes through the rock and radiative recombination on the backside.*

The UV-stimulated IR emission experiments were designed in such a way that the UV radiation hitting one surface of the sample would not transmit through the sample and not be able to reach the other surface from where the IR emission was measured. The rock samples were also thick enough that any Joule heat deposited into one surface by the intense UV beam would take relatively long time (minutes) to diffuse to the opposite side. As soon as the UV beam was turned on, however, we recorded a near-instantaneous change in the IR spectrum emitted from the far side of the sample. **Figure 18c** shows that this change occurs in two groups of emission bands (i) in the 750–950 cm^{-1} region and (ii) in the 1000–1300 cm^{-1} region of the spectrum. The group (i) is made of three bands at 925, 865 and 805 cm^{-1}. The group (ii) is made of three bands near 1030, 1100 and 1250 cm^{-1}. Though the assignment of these bands is still uncertain and will need more study, it is tempting to suggest that the origin of the groups (i) and (ii) bands is, in principle, the same as that of the IR emission bands, which we have deduced from rock deformation experiments during the summer of 2003.

In these rock deformation experiments a relatively small (10-12 cm diameter) cylindrical portion of large (30 x 60x 10 cm^3) blocks of anorthosite, a pure Ca-rich feldspar rock, were subjected to increasing levels of mechanical stress. As a result of the applied stress, p-hole charge carriers were activated in this "source volume". From electrical conductivity experiments carried out under similar conditions on the same rock we knew that the p-hole charge carriers were able to flow out of the "source volume" into the surrounding unstressed rock. Arriving at the surface the p-holes are expected to recombine, forming positive hole pairs, PHP.

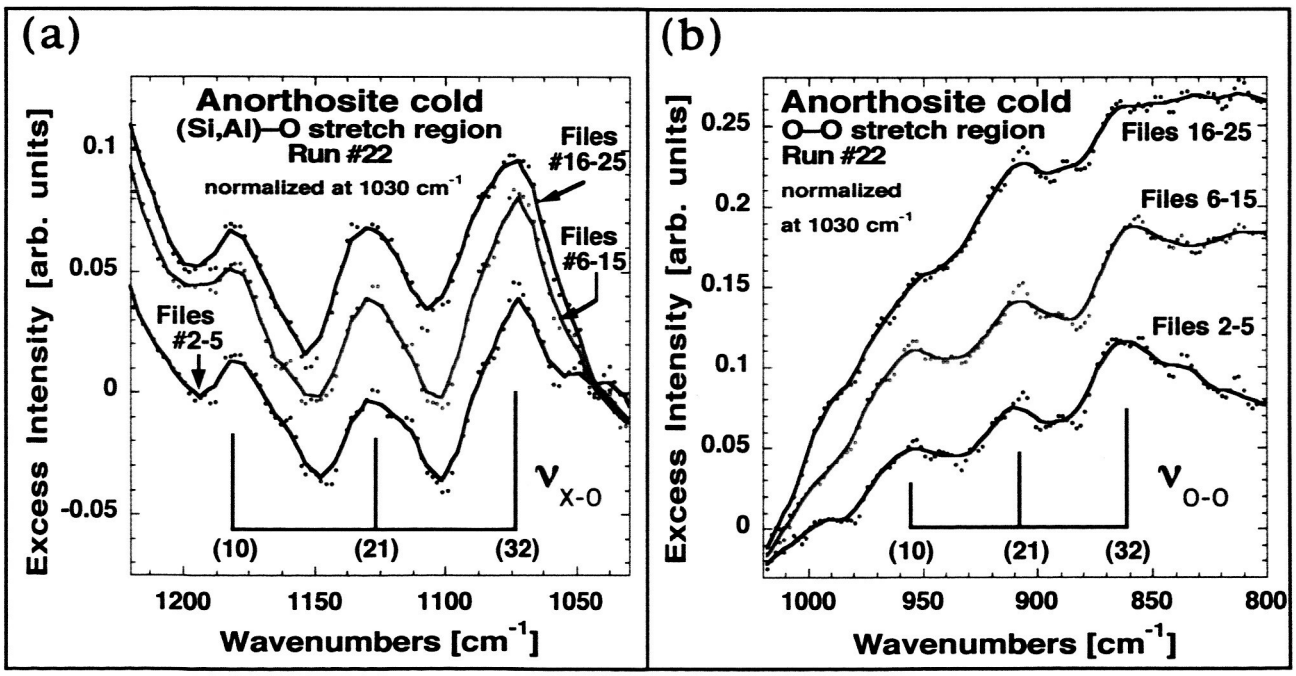

***Figure 19**: Excess IR emitted from the front of a slab of anorthosite rock, which was loaded 20-35 cm away. The IR emission spectrum suggests radiative recombination of p-holes activated in the stressed "source volume" and spreading out through the rock to the surface. **(a):** (Si-Al)–O stretching region and **(b)**: O-O stretching region with possible hot bands due to transitions between vibrationally excited states.*

The IR emission spectrum was recorded from the front end of the rocks, 20-35 cm away from the "source volume". **Figure 19a/b** shows the excess IR emission as obtained from the difference between the spectra "during deformation" minus "before deformation". **Figure 19a** covers the spectral range of the Si–O and Al–O stretching bands, while **Figure 19b** shows three bands at 955, 910 and 860 cm^{-1}, tentatively assigned to the vibrational deactivation of the highly excited O–O bonds that form upon the pairwise recombination of p-holes. The numbers in parenthesis (32), (21) and (10) indicate the transitions between

the quantum levels of the O–O vibrational manifold. Similarly, but equally uncertain at the present time, is the assignment of the three bands in the Si–O and Al–O stretching region to a non-radiative energy transfer from the highly excited O–O bonds into adjacent Si–O and Al–O bonds and their radiative decay.

Conclusion

The objectives set out for this work have been met by combining work performed under this relatively small grant with work performed under other grants. Strong experimental evidence has been obtained that both mechanical stress and hard UV irradiation lead to the activation of dormant electronic charge carriers in selected igneous rocks, that these charge carriers are p-holes, which are capable of propagating through the rock. Upon recombination at the rock surface the p-hole charge carriers appear to form vibrationally highly excited O–O bonds, which decay radiatively by emitting a series of O–O stretching bands and non-radiatively by channeling energy into adjacent Si–O and Al–O bonds, which in turn emit at their characteristic IR frequencies.

The results of the work performed or enabled under this proposal will form the basis for proposals to be submitted to other cognizant funding agencies.

References

Freund, F. (2002). "Charge generation and propagation in rocks." J. Geodynamics **33**(4-5): 545-572.

Freund, F., M. M. Freund and F. Batllo (1993). "Critical review of electrical conductivity measurements and charge distribution analysis of magnesium oxide." J. Geophys. Res. **98**(B12): 22209-22229.

Freund, F. T. (2003). "On the electrical conductivity structure of the stable continental crust." J. Geodynamics **35**: 353-388.

Hanson, D. R. and H. A. Spetzler (1994). "Transient creep in natural and synthetic, iron-bearing olivine single crystals: Mechanical results and dislocation microstructures." Tectonophys. **235**: 293-315.

Miguel, M. C., A. Vespignani, S. Zapperi, J. Weiss and J. R. Grasso (2001). "Intermittent dislocation flow in viscoplastic deformation." Nature **410**: 667-671.

Ricci, D., G. Pacchioni, M. A. Szymanski, A. L. Shluger and A. M. Stoneham (2001). "Modeling disorder in amorphous silica with embedded clusters: The peroxy bridge defect center." Physical Review B **64**(22): 224104-224101 - 224104-224108.

Takeuchi, A. and H. Nagahama (2001). "Voltage changes induced by stick-slip of granites." Geophys. Res. Lett. **28**(17): 3365-3368.

Vallianatos, F. and A. Tsanis (1998). "Electric current generation associated with the deformation rate of a solid: Preseismic and coseismic signals." Phys. Chem. Earth **23**: 933-938.

Wan, Z., Y. Zhang, X. Ma, M. D. King, J. S. Myers and X. Li (1999). "Vicarious calibration of the Moderate-Resolution Imaging Spectroradiometer Airborne Simulator thermal-infrared channels." Appl. Optics **38**(30): 6294-6306.